Journal of Molecular Graphics and Modelling 55 (2015) 33–40

Contents lists available at ScienceDirect

Journal of Molecular Graphics and Modelling

journal homepage: www.elsevier.com/locate/JMGM

Interlayer charge-transfer in impacting the second hyperpolarizabilities: Radical and cation species of hexathiophenalenylium and its nitro dimers

Li Wang, Wen-Yong Wang, Na-Na Ma, Dong-Mei Tian, Jiao Wang, Yong-Qing Qiu*

Institute of Functional Material Chemistry, Faculty of Chemistry, Northeast Normal University, Changchun, Jilin 130024, People's Republic of China

ARTICLE INFO

Article history:
Accepted 30 October 2014
Available online 7 November 2014

Keywords:
Dimer
Radical and cation
The second hyperpolarizability
Interlayer charge-transfer
DFT

ABSTRACT

Hexathiophenalenylium (HTPLY) has gained increasing attention for its interesting and potentially useful optical properties as a result of the enhancement in spin delocalization and charge-transfer of phenalenyl radicals, occasioned by the attachment of successive three disulfide linkages. Herein, we performed density functional theory to calculate the binding interactions, electronic absorption spectra and the second hyperpolarizabilities of cation and radical dimers of HTPLY and its nitro derivatives. It is found that the equilibrium structures of the π dimers at fully staggered position are most stable. Among these π dimers, radical dimers exhibit stronger binding interactions with respect to cation dimers. In addition, obvious red shifts in electronic spectra of radical dimers are dependent on the large interlayer charge-transfers. More importantly, radical dimers $^{3}[4]_{dim}$ and $^{1}[5]_{dim}$ exhibit a significant increase in the second hyperpolarizabilities as compared to cation dimers, which is due to lower excitation energies and larger interlayer charge-transfers. We believe that the results presented in this article shall provide important evidence for the large interlayer charge-transfers in enhancing the NLO properties of the π dimers.

1. Instruction

Various phenalenyl (PLY) based organic molecular materials have recently aroused widespread of both experimental and theoretical concerns owing to their intriguing and diverse properties in a wide range of electrical, optical, and magnetic properties [1–3]. The fascinating properties originate from the ability of interlayer self-association of PLY radical to form the π-dimer. Recent progress in PLY chemistry has led to the isolation of the radical in the crystalline state through the introduction of bulky substituents [4–8]. An increasing number of people have designed and pursued chalcogen substitution at the periphery of the PLY unit in order to obtain stable neutral radicals with less steric hindrance and further delocalization of an unpaired electron [9]. Chalcogens have been popular atoms for combination into the periphery of the molecular as a result of their contribution to strong interlayer interactions [10]. For example, Haddon et al. have synthesized crystallization of 1,9-dithiophenalenyl (DTPLY) with single disulfide-bridge that gives rise to a π-dimer [11]. This is the first example of a radical based on a single PLY unit that has been stabilized against σ-dimerization in the solid state by electronic effects rather than by the presence of sterically bulky substituents. Then soon, Haddon and co-workers demonstrated the presence of two disulfide groups in the tetrathiophenalenyl radical (TTPLY), which leads to a highly delocalized spin distribution and the lowest cell potential ever observed for a monofunctional PLY derivative [12].

Therefore, in principle, three dithio-bridged derivatives of PLY, named as hexathiophenalenylium (HTPLY), are possible. Thankfully, Haddon research group have successfully synthesized HTPLY and nitro-HTPLY cations and their π dimeric pairs [13]. They also reported an investigation into the effect of a disulfide bridge across two of the active positions of the PLY unit. The results show that these substituents electronically stabilize the free radical while sterically interfering with dimerization. The enhancement in spin delocalization of PLY radical is occasioned by the attachment of successive disulfide substituents [14,15]. On the other hand, interlayer delocalization between discrete monomers is originated from the ability of interlayer self-association of HTPLY radical to form the π-dimer.

The issue of designing molecular materials with intermolecule charge-transfer that exhibit large NLO responses have also been addressed both theoretically and experimentally [16–18]. However, few systematic studies have so far been performed on the

* Corresponding author. Tel.: +86 431 85099291; fax: +86 431 85098768.
E-mail address: qiuyq466@nenu.edu.cn (Y.-Q. Qiu).

http://dx.doi.org/10.1016/j.jmgm.2014.10.015
1093-3263/

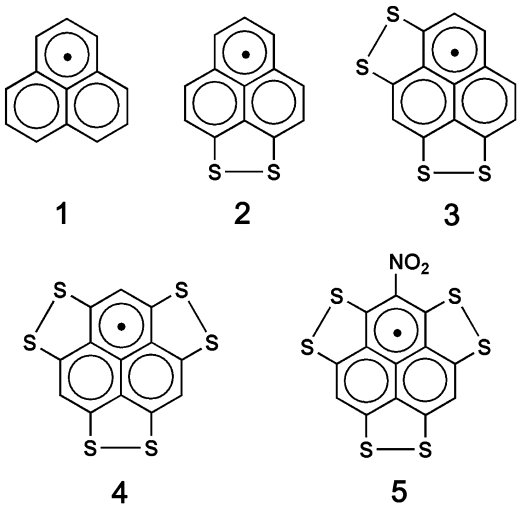

Fig. 1. Structures of radical monomers PLY (**1**), DTPLY (**2**), TTPLY (**3**), HTPLY (**4**), nitro-HTPLY (**5**).

second hyperpolarizabilities inside HTPLY and nitro-HTPLY π-dimers to investigate the relevant factors and, in particular, the role of intermolecule (interlayer) charge-transfer in affecting the NLO properties of the dimers. Continuing our interests in the study of the NLO responses of organic materials [19–21], in this work, we proceed theoretical studies on PLY (**1**), DTPLY (**2**), TTPLY (**3**), HTPLY (**4**), Nitro-HTPLY (**5**) monomers (Fig. 1). The synthetic cation dimers $[4]^{2+}_{dim}$, $[5]^{2+}_{dim}$ and corresponding radical dimers are mainly studied with the aim of researching their electronic structures, binding interactions, electronic absorption spectra and the second hyperpolarizabilities. It is interesting, then, to see interlayer charge-transfer transition in affecting the NLO properties of the π dimers. According to the theory of standpoint (Fig. 2), three possible electronic states, i.e., closed-sell states ($[4]_{dim}$ and $[5]_{dim}$), open-shell singlet states ($^1[4]_{dim}$ and $^1[5]_{dim}$), and open-shell triplet states ($^3[4]_{dim}$ and $^3[5]_{dim}$) will be considered during the radical dimers.

2. Computational details

According to previously reports, the ωB97XD functional is the long-range corrected hybrid density functional with damped atom–atom dispersion corrections, which appears most promising for calculations on π dimer systems [22]. And the hybrid meta exchange correlation functional M06-2X also performs well in calculations on π dimer systems [23]. Therefore, ωB97XD and M06-2X were selected to optimization of the geometries of the studied dimers. In addition, our calculations show that the optimized structure of $[4]^{2+}_{dim}$ and $[5]^{2+}_{dim}$ obtained by the ωB97XD functional is close to experimental results (see the related discussion in the geometrical structure section). As a result, the geometrical structures of the dimers were obtained at the ωB97XD/6-31+G (d) level of theory with all real frequencies.

In order to compare the strength of the dimerization sophisticatedly, the interaction energy (E_{int}) in dimers was also computed applying the same functional as for the optimization of the structures. To correct the basis set superposition error (BSSE), the counterpoise (CP) procedure was used to calculate the interaction energy qualitatively [24,25]. The interaction energy (E_{int}) can be expressed as the difference between the energy of the dimer and the sum of the energies of the monomers according to equation:

$$E_{int}(AB) = E(AB)_{AB} - [E(A)_{AB} + E(B)_{AB}] \quad (1)$$

It is well-known that the NLO properties are induced by nonlinear charge displacements that are generated under a strong electric field of light. In the presence of a weak and static electric field, the energy of a molecule is a function of the field strength. The energy of the perturbed system is described by the expansion [26,27].

$$E = E^0 - \mu_i F_i - \left(\frac{1}{2!}\right)\alpha_{ij}F_iF_j - \left(\frac{1}{3!}\right)\beta_{ijk}F_iF_jF_k - \left(\frac{1}{4!}\right)\gamma_{ijkl}F_iF_jF_kF_l + \ldots \quad (2)$$

where E^0 is the molecular energy in the absence of the applied electric field; μ_i is the molecular permanent dipole moment along the i direction; F_i is the Cartesian component of the applied electric field along the i direction; α_{ij}, β_{ijk} and γ_{ijkl} are the linear, first,

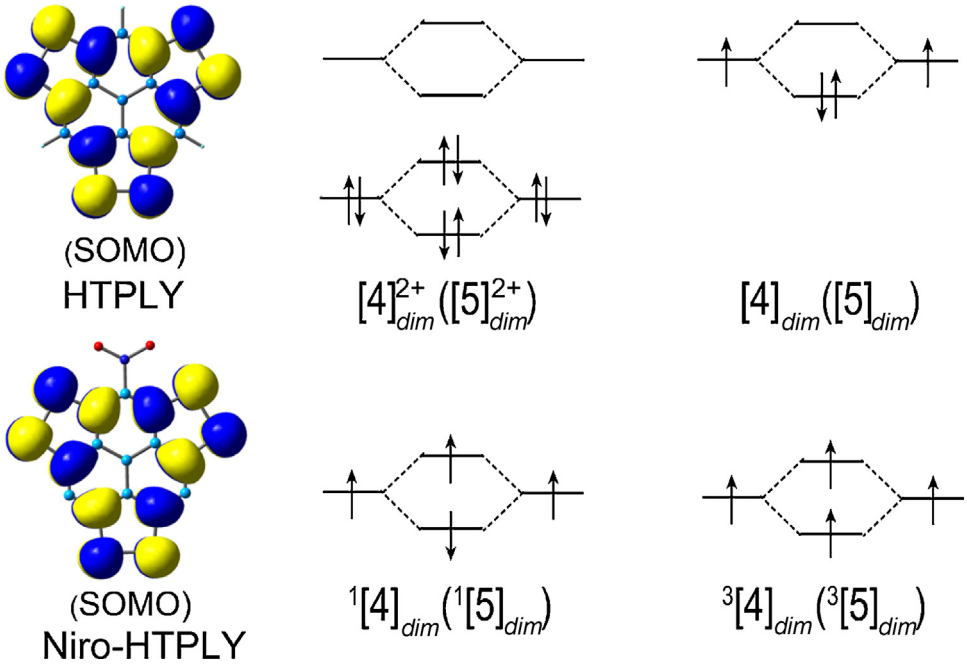

Fig. 2. The schematic occupancies of the two SOMOs in the dimers obtained at the ωB97XD/6-31+G (d, p) level of theory.

Table 1
Layer distances (L, Å) of the optimized structures and relative energies (E_{rel}, kcal/mol) of the radical dimers obtained by the ωB97XD functional.

Dimers	L	E_{rel}	Dimers	L	E_{rel}
$[4]^{2+}_{dim}$	3.406 (3.424[a], 3.201[b])	–	$[5]^{2+}_{dim}$	3.391 (3.394[a], 3.385[b])	–
$[4]_{dim}$	3.166	6.02	$[5]_{dim}$	3.257	13.55
$^1[4]_{dim}$	3.166	6.00	$^1[5]_{dim}$	3.384	0
$^3[4]_{dim}$	3.388	0	$^3[5]_{dim}$	3.382	0.30

[a] Experimental value.
[b] Layer distance obtained by M06-2X functional.

and second hyperpolarizability tensors, respectively; and *i*, *j*, and *k* designate the different components along the *x*, *y* and *z* directions, respectively.

When it comes to the calculation of (hyper)polarizabilities, three functionals have been chosen. The Coulomb-attenuated hybrid exchange-correlation (CAM-B3LYP) functional is a hybrid functional with improved long-range properties, which has been found to be more suitable functional for (hyper)polarizabilities calculations [28,29]. BHandHLYP functional, which includes a high percentage of HF exchange, successfully reduces the overestimation of the (hyper)polarizability [30] and reproduces the (hyper)polarizability values from the more sophisticated CCSD(T) method [31]. Moreover, the hybrid meta generalized gradient approximation (M06-2X) performs well for such π-stacking dimers [32].

To obtain more insight on the description of the trend of third-order NLO responses, the vertical electronic transition energies between the ground and excited states were simulated with time-dependent DFT (TD-DFT). It is know that TD-CAM-B3LYP functional is one of the most popular methods for the electron transition properties due to its efficiency and accuracy [33]. Therefore, the electron transition properties are computed as that used for the calculation of the second hyperpolarizabilities. Meanwhile, the electron–hole coherence of charge-transfer upon electronic transitions was investigated by means of the transition density matrix (TDM). The TDM were plotted using Multiwfn 3.2.60 [34].

All calculations in this work were carried out using Gaussian 09W package [35].

3. Results and discussion

3.1. Geometrical and electronic structure of dimer

All selected geometrical parameters are presented in Table 1 together with the X-ray crystal structures data of $[4]^{2+}_{dim}$ and $[5]^{2+}_{dim}$. In our optimized structures (Fig. 3) obtained by ωB97XD functional, the layer distances of $[4]^{2+}_{dim}$ and $[5]^{2+}_{dim}$ are 3.406 and 3.391 Å, which are very close to their experimental values of 3.424 and 3.394 Å. However, the layer distances of $[4]^{2+}_{dim}$ (3.201 Å) and $[5]^{2+}_{dim}$ (3.385 Å) obtained by M06-2X functional are generally smaller than those of the experimental values. It indicates that ωB97XD functional is very suitable for the optimizations of the HTPLY and nitro-HTPLY dimers. The optimized calculations of the studied dimers are performed at three possible spin states in order to find the structures with the lowest energies. The relative energies give a sequence for the stability of each radical dimers. It reveals that $^3[4]_{dim}$ and $^1[5]_{dim}$ show much lower energies than the other corresponding radical dimers. This stability is supported by the strong dimerization between two monomers in the latter discussion. Further, as compared to 3.406 Å of $[4]^{2+}_{dim}$, the layer distances of radical dimers $[4]_{dim}$, $^1[4]_{dim}$ and $^3[4]_{dim}$ are decreased to 3.166, 3.166, and 3.388 Å, respectively. Similar situations were also observed for $[5]_{dim}$, $^1[5]_{dim}$ and $^3[5]_{dim}$, indicating that the radical dimers are easier to have short interlayer distances. On the other hand, upon introduction of NO_2 to each dimer of $[4]^{2+}_{dim}$, the layer distance of $[5]^{2+}_{dim}$ decreases to 3.391 Å. It is also worth noting that interlayer distances of $[4]_{dim}$, $^1[4]_{dim}$ and $[5]_{dim}$ are significantly shorter than other dimers, which is due to the orbital–overlap contributions (which are described briefly below) (Fig. 4).

In order to make a reasonable explanation of the interlayer distances, the orbital distributions of molecular orbitals in the dimers will be taken into account. Orbital distributions of the highest occupied molecular orbitals (HOMOs) and the lowest unoccupied molecular orbitals (LUMOs) of all dimers have been probed in Fig. 5. As can be seen, for the singly occupied molecular orbitals (SOMO), there is no overlap between two mononers for cation dimers ($[4]^{2+}_{dim}$ and $[5]^{2+}_{dim}$), reflecting the small SOMO–SOMO overlap energetic component for the interaction. However, the HOMOs for $[4]_{dim}$, $^1[4]_{dim}$ and $[5]_{dim}$ have orbital–overlap contributions between two monomers. As a result of the orbital overlap, the layer distances of $[4]_{dim}$, $^1[4]_{dim}$ and $[5]_{dim}$ becomes small. Moreover, it is generally believed that low-lying HOMO–LUMO energy gap might be helpful for enhancing the second hyperpolarizability of molecular. The HOMO–LUMO energy gaps of the radical dimers are observably smaller than the cation dimers (Table 2). Thus, severe increases of the second hyperpolarizabilities values are expected for the radical dimers.

A further step into the potential energy curve was taken in order to elucidate the origin of the stabilities of these dimers. As a prototypical example of these types of dimers, potential energy curves of $[4]^{2+}_{dim}$ are given in Fig. 5. To examine the stability of $[4]^{2+}_{dim}$ as compared to the stretching motion of two monomers, two monomers are artificially pulled or pushed with the change of the layer distance L. The relationship between the distance *L* and E_{rel} of the model structure with respect to the equilibrium structure is exhibited in Fig. 5(a). As is shown, E_{rel} of the model structure at L = 5.406 Å is about 20 kcal/mol higher than the corresponding value of the equilibrium structure, which indicates that the stability of $[4]^{2+}_{dim}$ upon the stretching motion of two monomers. Additionally, the stability of $[4]^{2+}_{dim}$ at fully staggered position should be examined with respect to the rotating motion of two monomers. In the model structure, two monomers are artificially rotated along the perpendicular axis through the center of the monomer. The potential energy curve of the rotation angle θ is exhibited in Fig. 5(b). E_{rel} (17.27 kcal/mol) of $[4]^{2+}_{dim}$ at fully eclipsed position is the largest at an angle θ of about 60°, which is quite larger than that (about 0 kcal/mol) at fully staggered position and means that the studied dimer at fully staggered position is reasonable.

3.2. Binding interaction of dimer

It is visualized from Table 2 that the E_{int} for $[4]^{2+}_{dim}$ (27.24 kcal/mol) and $[5]^{2+}_{dim}$ (25.24 kcal/mol) are positive value,

Table 2
Interaction energies (E_{int}, kcal/mol) and HOMO–LUMO energy gaps (E_{gap}, eV) of the dimers calculated at the ωB97XD/6-31+G (d, p) level of theory.

Dimers	E_{int}	E_{gap}	Dimers	E_{int}	E_{gap}
$[4]^{2+}_{dim}$	27.24	5.70	$[5]^{2+}_{dim}$	25.24	5.78
$[4]_{dim}$	−19.28	3.64	$[5]_{dim}$	−9.65	3.18
$^1[4]_{dim}$	−19.29	3.64	$^1[5]_{dim}$	−22.37	4.34
$^3[4]_{dim}$	−25.39	5.19	$^3[5]_{dim}$	−22.05	4.26

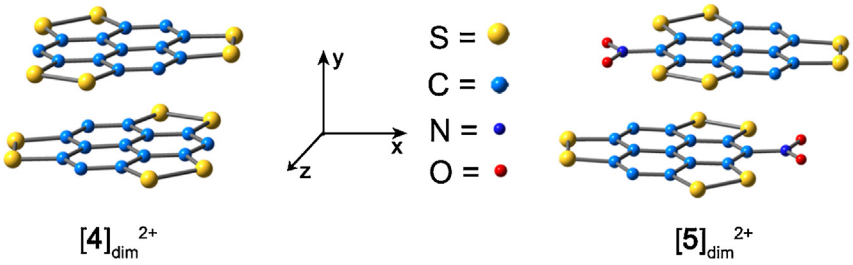

Fig. 3. Molecular structure formulas of the dimers.

which may be due to the large electrostatic repulsion between two monomers with positive charges. While for radical dimers, the E_{int} values are negative, supporting their strong interaction energies. Therefore, the radical dimers show high thermal and chemical stabilities. Moreover, the strong binding interactions are beneficial for the stability of the dimerization. For radical dimers of HTPLY with different spin states, the absolute E_{int} values follow the trend: 25.39 kcal/mol ($^3[4]_{dim}$) > 19.29 kcal/mol ($^1[4]_{dim}$) > 19.28 kcal/mol ($[4]_{dim}$). It indicates that $^3[4]_{dim}$ exhibits the strongest binding interaction and thus is most stable. While for radical dimers of Niro-HTPLY, the absolute values of E_{int} follow the trend: 22.37 kcal/mol ($^1[5]_{dim}$) > 22.05 kcal/mol ($^3[5]_{dim}$) > 9.65 kcal/mol ($[5]_{dim}$), indicating that $^1[5]_{dim}$ is most stable. Thus, in terms of structures with stable spin states, their electronic absorption spectra and the second hyperpolarizabilities will be further studied.

3.3. Electronic absorption spectrum

The electronic absorption spectra of cation and most stable radical dimers were calculated by TD-CAM-B3LYP functional with 50 excited states. The calculation shows excellent convergence property. Because increasing the numbers of excited states of $[4]^{2+}_{dim}$ to 100 states has no impact on the low-energy excitation with exception of very slightly effect on the high-energy excitation (Fig. S1 in supporting information), indicating that the low-energy excitation with 50 excited states has been well described. Since, the main research of our goal is the low-energy region, TDDFT calculation with 50 excited states was enough for the research of UV–vis spectroscopy. The electronic absorption spectra of all dimers show two intense bands in the UV–vis region: high-energy and low-energy peaks (Fig. 6). According to the simulated spectra, the high-energy peak of $[4]^{2+}_{dim}$, $^3[4]_{dim}$, $[5]^{2+}_{dim}$ and $^1[5]_{dim}$ are at 275.8 nm, 385.0 nm, 333.1 nm and 377.6 nm. The low-energy absorption peak of $[4]^{2+}_{dim}$, $^3[4]_{dim}$, $[5]^{2+}_{dim}$ and $^1[5]_{dim}$ are at 402.0 nm, 566.7 nm, 420.3 nm and 724.1 nm, respectively. It is interesting to note that remarkable bathochromic-shifts are observed in radical dimers $^3[4]_{dim}$ and $^1[5]_{dim}$, as compared with $[4]^{2+}_{dim}$ and $[5]^{2+}_{dim}$. And the bathochromic-shift will exhibit relatively high values of the second hyperpolarizabilities.

3.4. The static second hyperpolarizability

3.4.1. The second hyperpolarizability of monomer

The second hyperpolarizabilities (γ) of **1**, **2**, **3**, **4** and **5** monomers were calculated using the CAM-B3LYP functional. The results show that the γ values of these monomers follow the trend: 2.8×10^5 au (**5**) > 2.3×10^5 au (**4**) > 2.2×10^5 au (**3**) > 1.3×10^5 au (**2**) > 6.4×10^4 au (**1**). It indicates that increasing the numbers of disulfide groups is helpful for enhancing the second hyperpolarizability of molecular. Due to the larger γ values of the **4** and **5** monomers, we have focused on the second hyperpolarizabilities of π-dimers of **4** and **5** for finding enhanced NLO materials.

3.4.2. The second hyperpolarizability of dimer

In order to investigate the polarization along the dimeric direction, the second hyperpolarizabilities (γ_{yyyy}) of $[4]^{2+}_{dim}$, $^3[4]_{dim}$, $[5]^{2+}_{dim}$ and $^1[5]_{dim}$ have been mainly listed in Table 3. Considering the influence of the DFT methods on the NLO responses, the γ_{yyyy} values were calculated using the CAM-B3LYP, BHandHLYP, and M06-2X functionals based on the same geometries. The results show that the γ values obtained using different functionals are very close for the same dimer, and the three functionals display the same trends in the γ_{yyyy} values for the studied dimers. To discuss these results in more detail, we use the data from the CAM-B3LYP functional to evaluate the order of the γ_{yyyy} values for the dimers. The γ_{yyyy} values of $^3[4]_{dim}$ and $^1[5]_{dim}$ are ~2.8 and ~17.1 times larger

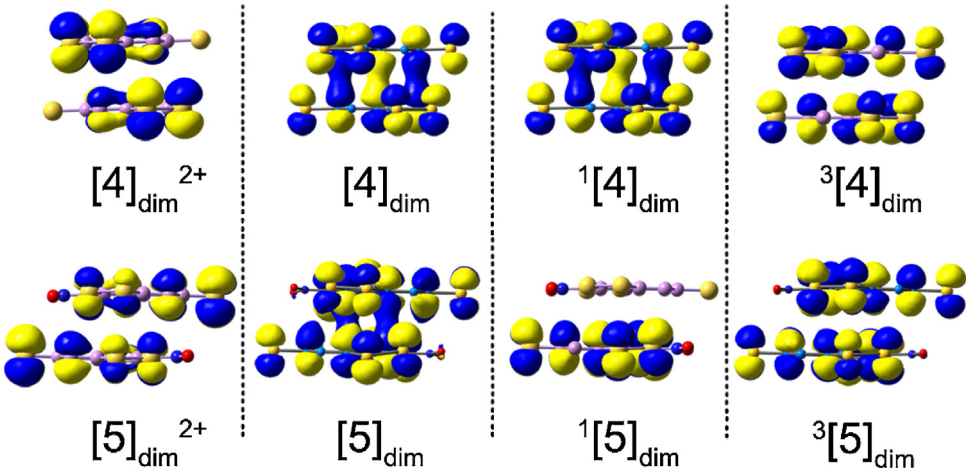

Fig. 4. The electronic distribution of HOMOs of the dimers.

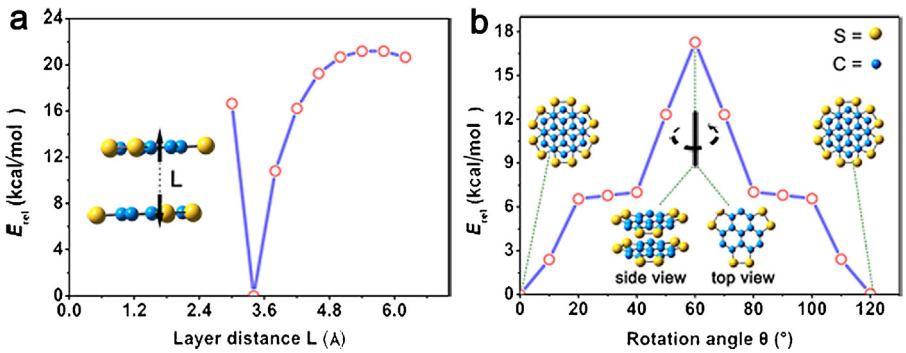

Fig. 5. The mechanical stability of $[4]^{2+}_{dim}$ with respect to the (a) stretching and (b) rotating motion of the monomer.

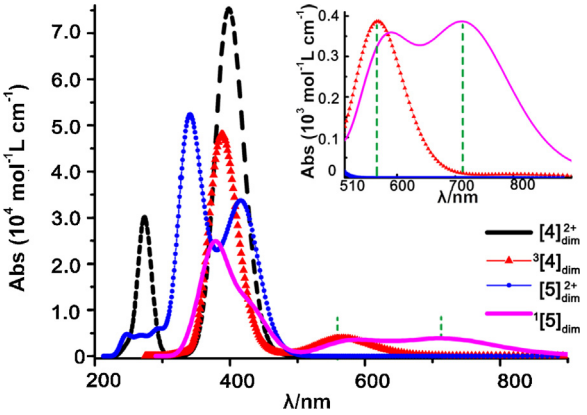

Fig. 6. Electronic absorption spectra of $[4]^{2+}_{dim}$, $^3[4]_{dim}$, $[5]^{2+}_{dim}$ and $^1[5]_{dim}$ computed by TD-CAM-B3LYP/6-31+G (d, p).

than that of $[4]^{2+}_{dim}$ and $[5]^{2+}_{dim}$, which is due to the addition of an additional electron to each monomer to form radical dimers. It is no doubt that the radical dimers with the larger interaction energy and lower energy gap have a considerable enhancement of the γ_{yyyy} values with respect to cation dimers. The γ_{yyyy} value of $^1[5]_{dim}$ is ~6.0 times as large as $^3[4]_{dim}$, which indicates that the introduction of the strong electron-withdrawing substituent on the HTPLY is helpful to increase the γ_{yyyy} values. In addition, $[1]^{2+}_{dim}$ (cation dimer of PLY) and $^3[1]_{dim}$ (triplet state of PLY radical dimer) have been added into Table 3. The second hyperpolarizability (γ_{yyyy}) of $^3[1]_{dim}$ is comparable to that obtained by Zhong, etc. (J. Chem. Phys. 139 (2013) 124314). In addition, the results show that the γ_{yyyy} values of $[4]^{2+}_{dim}$ and $[5]^{2+}_{dim}$ are very close to that of $[1]^{2+}_{dim}$. However, the γ_{yyyy} values of $^3[4]_{dim}$ and $^1[5]_{dim}$ are ~3.0 times and ~18.3 times as large as $^3[1]_{dim}$. It means that the studied radical dimers in the revised manuscript have larger γ_{yyyy} values than representative radical dimer, indicating that the third-order nonlinear optical effects have been improved.

To have an insight into the origin of third-order NLO responses and to explain the effect of three dithio-bridges on NLO responses, two-level model of the second hyperpolarizability (γ) is considered for the studied Dimers, which is the linkage between the γ and electronic transition(s) in low-lying crucial excited states. Therefore, using the two-level models [36] is a reliable way to analyze second hyperpolarizabilities of molecules and the expression is as follows:

$$\gamma \propto \frac{f_{gm}^2}{E_{gm}^5} \tag{3}$$

where f_{gm} is the oscillator strength, and E_{gm} is the transition energy. In the two-level expression, the γ value is proportional to the quadratic power of f_{gm} but inversely proportional to the fifth power of E_{gm}. Hence, E_{gm} might be considered as the decisive factor in the second hyperpolarizability. The excited state E_{gm} (eV), and relevant molecular orbitals of $[4]^{2+}_{dim}$, $^3[4]_{dim}$, $[5]^{2+}_{dim}$ and $^1[5]_{dim}$ in singlet excited-state transitions are summarized in Table 4. For the low-lying crucial excited states, the transition energy order of dimers decreases as: 3.08 eV ($[4]^{2+}_{dim}$) > 2.95 eV ($[5]^{2+}_{dim}$) > 2.19 eV ($^3[4]_{dim}$) > 1.71 eV ($^1[5]dim$), which is in quantitative agreement (inversely proportional) with the order of their increasing γ_{yyyy} values (Fig. 7). On the basis of this order of E_{gm}, $^3[4]_{dim}$ and $^1[5]_{dim}$ with lower transition energies present larger γ_{yyyy} values, with respect to $[4]^{2+}_{dim}$ and $[5]^{2+}_{dim}$. On the other hand, the incorporation of the strong electron-withdrawing NO_2 group results in the decrease of transition energies (the E_{gm} of $[5]^{2+}_{dim}$ and $^1[5]_{dim}$ are smaller than $[4]^{2+}_{dim}$ and $^3[4]_{dim}$, respectively), thus the γ_{yyyy} values are enhanced.

Following, the charge-transfer transition properties of the crucial excited states (Fig. 8), which distribute mostly to the NLO responses, were considered. The low-energy electronic transition of $[4]^{2+}_{dim}$ arises from HOMO-2 → LUMO. Additionally, the two monomers contribute equally to the HOMO-2 and LUMO and there is no overlap between the orbitals of HOMO-2 and LUMO, reflecting that the interlayer charge-transfer transition may be slight. The

Table 3
The absolute values of second hyperpolarizabilitties along the dimeric direction (γ_{yyyy}) (10^4 au) of $[1]^{2+}_{dim}$, $^3[1]_{dim}$, $[4]^{2+}_{dim}$, $^3[4]_{dim}$, $[5]^{2+}_{dim}$ and $^1[5]_{dim}$ obtained by the CAM-B3LYP, M06-2X and BHandHLYP functionals.

Dimers	Functionals	γ_{yyyy}	Dimers	Functionals	γ_{yyyy}
$[1]^{2+}_{dim}$	CAM-B3LYP	7.6	$^3[1]_{dim}$	CAM-B3LYP	6.1
	M06-2X	5.9		M06-2X	5.9
	BHandHLYP	6.1		BHandHLYP	6.1
$[4]^{2+}_{dim}$	CAM-B3LYP	6.7	$^3[4]_{dim}$	CAM-B3LYP	18.5
	M06-2X	7.5		M06-2X	24.9
	BHandHLYP	6.5		BHandHLYP	16.7
$[5]^{2+}_{dim}$	CAM-B3LYP	6.5	$^1[5]_{dim}$	CAM-B3LYP	111.4
	M06-2X	6.8		M06-2X	66.7
	BHandHLYP	6.4		BHandHLYP	77.3

Table 4
Excited transition energies (E_{gm}, eV), absorption wavelength (λ_{gm}, nm) at low-energy peak, and major molecular orbital contributions of the dimers calculated at the CAM-B3LYP/6-31+G (d, p) level.

Dimers	λ_{gm}	E_{gm}	MO transitions
$[4]^{2+}_{dim}$	401.9	3.08	H[a]-2 → L (93%)
$^3[4]_{dim}$	566.7	2.19	αH → αL+10 (53%), αH-1 → αL+6 (26%)
$[5]^{2+}_{dim}$	420.3	2.95	H → L+1 (53%), H-1 → L (34%),
$^1[5]_{dim}$	724.1	1.71	αH → αL+1 (43%), βH → βL+1 (43%)

[a] H = HOMO, H-1 = HOMO-1, L = LUMO, L+1 = LUMO, etc.

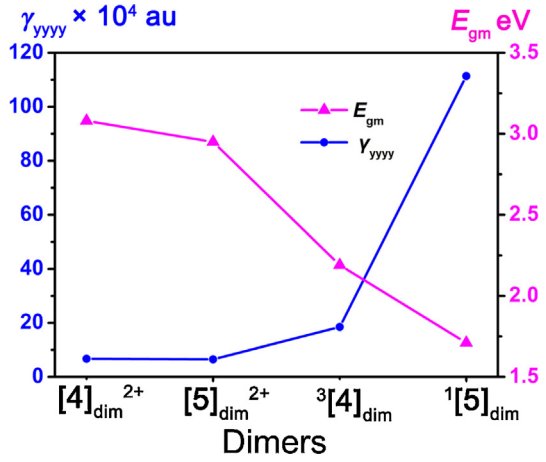

Fig. 7. Relationship between the γ_{yyyy} values and the corresponding E_{gm} values for the four dimers.

electronic transition of $[5]^{2+}_{dim}$ is associated with HOMO → LUMO+1 and HOMO-1 → LUMO excitations and there is orbital overlap between the orbital of LUMO. As a result, the charge-transfer transition of $[5]^{2+}_{dim}$ consists not only of intralayer charge-transfer, but also a little interlayer charge-transfer transition. Upon insertion of an additional electron to each monomer of $[4]^{2+}_{dim}$, the electronic transition of $^3[4]_{dim}$ is associated with αHOMO → αLUMO+10 and αHOMO-1 → αLUMO+6 excitations and there are overlaps between orbitals of αLUMO+10 and αLUMO+6, thus the interlayer charge-transfer transition may be present. The radical dimer $^1[5]_{dim}$ can be viewed to be formed from $^3[4]_{dim}$ by adding two NO_2 groups at the terminal sites along the *x*-axis. The electronic transition of $^1[5]_{dim}$ is associated with αHOMO → αLUMO+1 and βHOMO → βLUMO+1 excitations. All these transitions are obvious due to the large overlap between the orbitals of HOMOs, which is responsible for the enhanced γ_{yyyy} of $^3[4]_{dim}$ and $^1[5]_{dim}$.

However, taking into account the shape of the molecular orbitals merely is not sufficient to determine whether the electronic transitions occurred within the two respective monomers or between the two monomers. Whereas, TDM is a helpful tool for analyzing electronic excitation processes and providing additional information on electron–hole localization and coherence of specific excitation [37]. Therefore, plotting the TDM as a color-filled map is especially useful for visually studying the charge-transfer patterns of the low-energy peak. The hydrogen atoms have been omitted since they usually have little contribution to the transitions in the TDM.

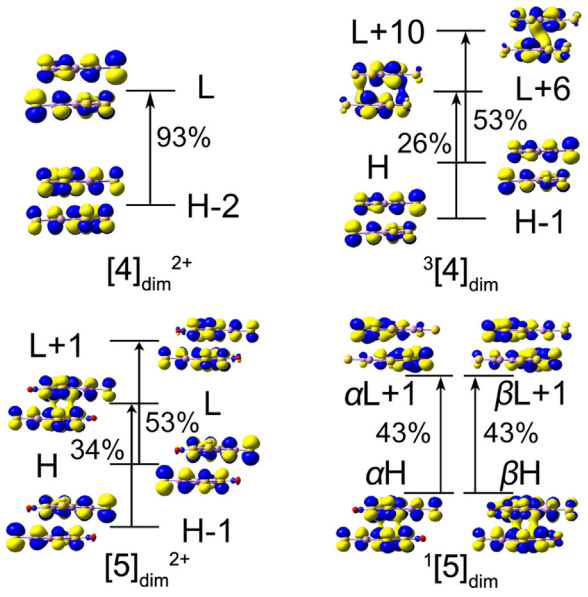

Fig. 8. Orbital diagrams of $[4]^{2+}_{dim}$, $[5]^{2+}_{dim}$, $^3[4]_{dim}$ and $^1[5]_{dim}$ involved in the dominant electron transition (H = HOMO, H-1 = HOMO-1, L = LUMO, L+1 = LUMO, etc.).

Inspection of $[4]^{2+}_{dim}$ and $[5]^{2+}_{dim}$ (Fig. 9) reveals that the low-energy electronic transitions could be assigned as intralayer charge-transfers within the two respective monomers along with less interlayer charge-transfer character between the two monomers, since the electron–hole pairs are mainly localized along the diagonal element and still a little delocalized along the off-diagonal element. Note that the electron–hole coherence associated with the low-energy peak of $[4]^{2+}_{dim}$ and $[5]^{2+}_{dim}$ is mainly delocalized on the whole molecule (along the diagonal element), demonstrating the intralayer delocalized transition. Besides, there is still a little correlation seen in the off-diagonal element, which points to the small probability of interlayer charge-transfer between the two monomers. While, the electron–hole pairs of $^3[4]_{dim}$ and $^1[5]_{dim}$ are mainly localized both along the diagonal element and the off-diagonal element. Therefore, the charge-transfers of $^3[4]_{dim}$ and $^1[5]_{dim}$ are the mixture of intralayer charge-transfers within the two respective monomers coupled with charge-transfers between the two monomers in a great degree. The enhanced interlayer charge-transfers in $^3[4]_{dim}$ and $^1[5]_{dim}$ bring about much stronger polarizations of HTPLY and nitro-HTPLY monomers with respect to $[4]^{2+}_{dim}$ and $[5]^{2+}_{dim}$. The polarizations lead to strong enhancement of the γ_{yyyy} values of $^3[4]_{dim}$ and $^1[5]_{dim}$ when compared to $[4]^{2+}_{dim}$ and $[5]^{2+}_{dim}$. This is also supported by the substantial changes of transition energies, that $^3[4]_{dim}$ and $^1[5]_{dim}$ exhibits lower transition energies than $[4]^{2+}_{dim}$ and $[5]^{2+}_{dim}$. Apparently, the enhanced interlayer charge-transfers in $^3[4]_{dim}$ and $^1[5]_{dim}$ result in the red-shift of the low-energy absorption spectrum upon comparison with those of $[4]^{2+}_{dim}$ and $[5]^{2+}_{dim}$.

In the above dimers, the low-energy peaks can be assigned to the mixture of intralayer charge-transfer within the respective monomers and interlayer charge-transfer between the two monomers. The obvious interlayer charge-transfers of $^3[4]_{dim}$ and $^1[5]_{dim}$ are due to the large overlap between the orbitals of HOMOs and LUMOs, which is responsible for the enhanced γ_{yyyy} values of radical dimers with respect to cation dimers ($[4]^{2+}_{dim}$ and $[5]^{2+}_{dim}$). In the case of $^3[4]_{dim}$ and $^1[5]_{dim}$, the interlayer orbital overlap provides the pathway for the redistribution of electronic charges, while unpaired electrons serve as charge carriers. As a result, the radical dimers have the remarkable interlayer charge-transfers, which give rise to the enhanced γ_{yyyy} values as compared to the cation dimers.

3.4.3. *The frequency-dependent second hyperpolarizability of dimer*

The frequency-dependent second hyperpolarizabilities of Kerr effect (EOKE) γ ($-\omega$, ω, 0, 0) and electric-field induced second harmonic (EFISH) γ (-2ω, ω, ω, 0) of dimer $[4]^{2+}_{dim}$ (along the dimeric direction) have been investigated by coupled-perturbed DFT at CAM-B3LYP/6-31+G (d,p) level. The calculated results are listed in Table S1 (Supporting Information). Generally, the molecular hyperpolarizabilities, γ (-2ω, ω, ω, 0), have been measured in a fundamental incident wavelength which has a second harmonic far enough from the absorption bands to avoid the over measurement of γ values due to resonance effects. Hence, according to the maximum absorption of $[4]^{2+}_{dim}$ at about 402 nm, we investigated the frequency dispersion at a near resonant wavelength of 1.340 mm (ω = 0.0340 au) and a nonresonant wavelength of 1.907 mm (ω = 0.0239 au). The results show that the frequency dependent values γ (-2ω, ω, ω, 0) are 7.1×10^4 au and 7.6×10^4 au

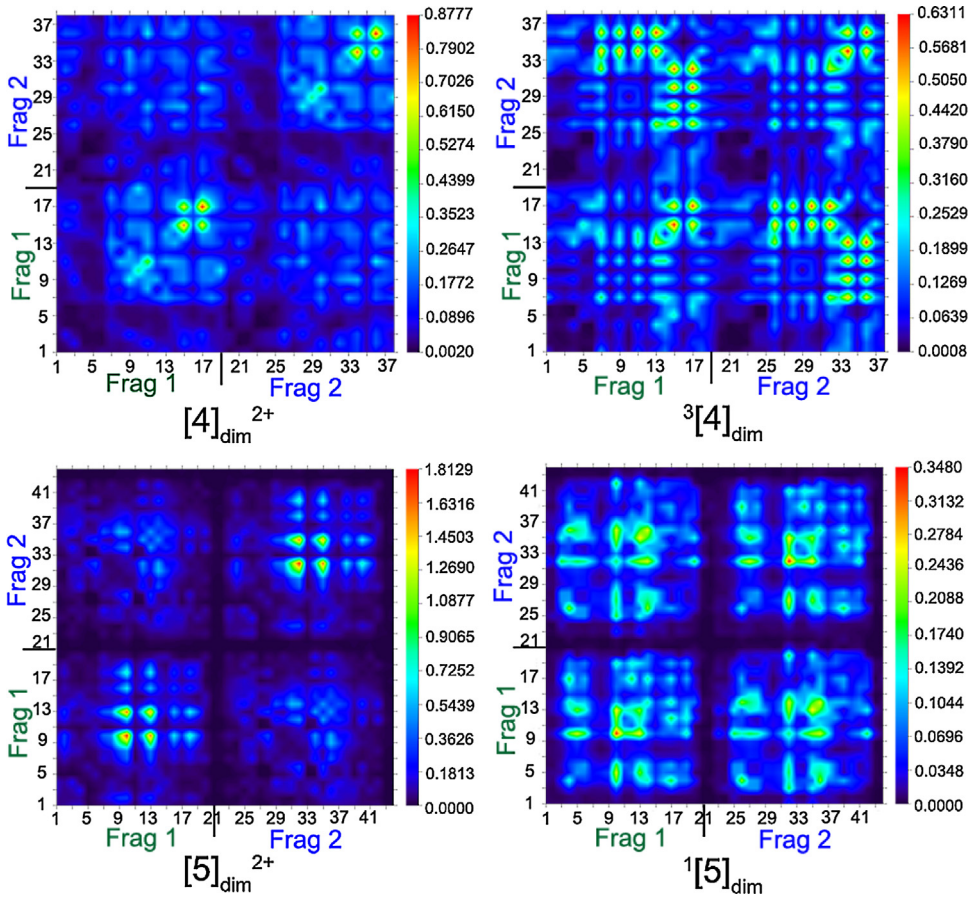

Fig. 9. The TDM corresponding to the low-energy electronic transitions of dimers $[4]^{2+}_{dim}$, $[5]^{2+}_{dim}$, $^{3}[4]_{dim}$ and $^{1}[5]_{dim}$ (upper layer of the dimer is named Frag 1, while the lower layer is Frag 2).

(increasing by about 6% at $\omega = 0.0239$ au and 13% at $\omega = 0.0340$ au, respectively). While the γ $(-\omega, \omega, 0, 0)$ values are 6.9×10^4 au and 7.0×10^4 au (increasing by about 3% at $\omega = 0.0239$ au and 4% at $\omega = 0.0340$ au, respectively). It indicates that the dispersion behavior of EFISH and EOKE on the second hyperpolarizabilities are relatively weak for the studied dimer.

4. Conclusion

The present study reveals that the thermal stability of radical dimers of HTPLY and Niro-HTPLY units is greater with respect to the corresponding cation dimers. On the basis of the strong binding interactions between the two monomers of radical dimers, it can be concluded that the interlayer interactions add further supports to the thermal stabilities of π dimers and the large interlayer charge-transfers induce longer wavelength absorption in visible area. The noteworthy enhancement of γ_{yyyy} values for radical dimers with respect to cation dimers has been satisfactorily rationalized in terms of the spectroscopic properties relevant to the low-energy electronic transitions and large interlayer charge-transfers. This work may provide a notable contribution for designing and synthesizing excellent NLO materials by virtue of their strong binding interactions, low-excitation energies and large interlayer charge-transfers. It is expected that the results will simulate experimental research on the NLO properties of π dimeric pairs of HTPLY.

Acknowledgment

This work was supported by the Natural Science Foundation of China (No. 21173035).

Appendix A. Supplementary data

Supplementary data associated with this article can be found, in the online version, at http://dx.doi.org/10.1016/j.jmgm.2014.10.015.

References

[1] J. Huang, M. Kertesz, Spin crossover of spiro-biphenalenyl neutral radical molecular conductors, J. Am. Chem. Soc. 125 (2003) 13334–13335.
[2] S.K. Mandal, M.E. Itkis, X. Chi, S. Samanta, D. Lidsky, R.W. Reed, New family of aminophenalenyl-based neutral radical molecular conductors: synthesis, structure, and solid state properties, J. Am. Chem. Soc. 127 (2005) 8185–8196.
[3] S.K. Pal, M.E. Itkis, F.S. Tham, R.W. Reed, R.T. Oakley, B. Donnadieu, Phenalenyl-based neutral radical molecular conductors: substituent effects on solid-state structures and properties, J. Am. Chem. Soc. 129 (2007) 7163–7174.
[4] M.E. Itkis, X. Chi, A.W. Cordes, R.C. Haddon, Magneto-opto-electronic bistability in a phenalenyl-based neutral radical, Science 296 (2002) 1443–1445.
[5] A. Shimizu, M. Uruichi, K. Yakushi, H. Matsuzaki, H. Okamoto, M. Nakano, Resonance balance shift in stacks of delocalized singlet bi-radicals, Angew. Chem. Int. Ed. 48 (2009) 5482–5486.
[6] Y. Morita, T. Aoki, K. Fukui, S. Nakazawa, K. Tamaki, S. Suzuki, A new trend in phenalenyl chemistry: a persistent neutral radical, 2,5,8-tri-tert-butyl-1,3-diazaphe-nalenyl, and the excited triplet state of the gable syn-dimer in the crystal of column motif, Angew. Chem. Int. Ed. 41 (2002) 1793–1796.
[7] F. Mota, J.S. Miller, J.J. Novoa, Comparative analysis of the multicenter, long bond in $[TCNE]^{-}$ and phenalenyl radical dimers: a unified description of multicenter, long bonds, J. Am. Chem. Soc. 131 (2009) 7699–7707.
[8] Z.H. Cui, H. Lischka, H.Z. Beneberu, M. Kertesz, Rotational barrier in phenalenyl neutral radical dimer: separating pancake and van der Waals interactions, J. Am. Chem. Soc. 136 (2014) 5539–5542.
[9] A. Mailman, S.M. Winter, X. Yu, C.M. Robertson, W. Yong, J.S. Tse, Crossing the insulator-to-metal barrier with a thiazyl radical conductor, J. Am. Chem. Soc. 134 (2012) 9886–9889.
[10] F. Wudl, From organic metals to superconductors: managing conduction electrons in organic solids, Acc. Chem. Res. 17 (1984) 227–232.

[11] L. Beer, S.K. Mandal, R.W. Reed, R.T. Oakley, F.S. Tham, B. Donnadieu, The first electronically stabilized phenalenyl radical: effect of substituents on solution chemistry and solid-state structure, Cryst. Growth Des. 7 (2007) 802–809.
[12] L. Beer, R.W. Reed, C.M. Robertson, R.T. Oakley, F.S. Tham, R.C. Haddon, Tetrathiophenalenyl radical and its disulfide-bridged dimer, Org. Lett. 10 (2008) 3121–3123.
[13] R.C. Haddon, S.V. Chichester, S.M. Stein, J.H. Marshall, A.M. Mujsce, Perchloro-7H-cycloprop[a]acenaphthylene and the perchlorophenalenyl system, J. Org. Chem. 52 (1987) 711–712.
[14] P. Bag, F.S. Tham, B. Donnadieu, R.C. Haddon, Hexathiophenalenylium cations: syntheses, structures, and redox chemistry, Org. Lett. 15 (2013) 1198–1201.
[15] R.C. Haddon, F. Wudl, M.L. Kaplan, J.H. Marshall, R.E. Cais, F.B. Bramwell, 1,9-Dithiophenalenyl system, J. Am. Chem. Soc. 100 (1978) 7629–7633.
[16] P.G. Lacroix, T. Hayashi, T. Sugimoto, K. Nakatani, V. Rodriguez, Optical nonlinearity in (EDT-DSDTFVO) 2·FeBr4, an intriguing molecular material with metallic conductivity, magnetoresistance effects, and quadratic nonlinear optical properties, J. Phys. Chem. C 114 (2010) 21762–21769.
[17] J. Zyss, I. Ledoux, S. Volkov, V. Chernyak, S. Mukamel, G.P. Bartholomew, Through-space charge transfer and nonlinear optical properties of substituted paracyclophane, J. Am. Chem. Soc. 122 (2000) 11956–11962.
[18] J.F. Lamère, I. Malfant, A. Sournia-Saquet, P.G. Lacroix, J.M. Fabre, L. Kaboub, Quadratic nonlinear optical response in partially charged donor-substituted tetrathiafulvalene: from a computational investigation to a rational synthetic feasibility, Chem. Mater. 19 (2007) 805–815.
[19] W.Y. Wang, N.N. Ma, S.L. Sun, Y.Q. Qiu, Impact of redox stimuli on ferrocene–buckybowl complexes: switchable optoelectronic and nonlinear optical properties, Organometallics 33 (2014) 3341–3352.
[20] W.Y. Wang, N.N. Ma, C.H. Wang, M.Y. Zhang, S.L. Sun, Y.Q. Qiu, Enhancement of second-order nonlinear optical response in boron nitride nanocone: Li-doped effect, J. Mol. Graph. Model. 48 (2014) 28–35.
[21] X.X. Sun, N.N. Ma, X.J. Li, S.L. Sun, H.M. Xie, Y.Q. Qiu, Computational study: how redox affect the nonlinear optical properties of donor substituted heteroleptic bis-tridentate Ru(II) complexes? J. Mol. Graph. Model. 38 (2012) 248–255.
[22] L.M. da Costa, S.R. Stoyanov, S. Gusarov, X. Tan, M.R. Gray, J.M. Stryker, Density functional theory investigation of the contributions of π–π stacking and hydrogen-bonding interactions to the aggregation of model asphaltene compounds, Energy Fuels 26 (2011) 2727–2735.
[23] R.L. Zhong, J. Zhang, S. Muhammad, Y.Y. Hu, H.L. Xu, Z.M. Su, Boron/nitrogen substitution of the central carbon atoms of the biphenalenyl diradical π dimer: a novel 2e–12c bond and large NLO responses, Chem. Eur. J. 17 (2011) 11773–11779.
[24] I. Alkorta, J. Elguero, Theoretical study of strong hydrogen bonds between neutral molecules: the case of amine oxides and phosphine oxides as hydrogen bond acceptors, J. Phys. Chem. A 103 (1998) 272–279.
[25] S.F. Boys, F. Bernardi, The calculation of small molecular interactions by the differences of separate total energies: some procedures with reduced errors, Mol. Phys. 19 (1970) 553–566.
[26] N.N. Ma, S.L. Sun, C.G. Liu, X.X. Sun, Y.Q. Qiu, Quantum chemical study of redox-switchable second-order nonlinear optical responses of D–π–A system BNbpy and metal Pt(II) chelate complex, J. Phys. Chem. A 115 (2011) 13564–13572.
[27] W.Y. Wang, X.F. Du, N.N. Ma, S.L. Sun, Y.Q. Qiu, Theoretical investigation on switchable second-order nonlinear optical (NLO) properties of novel cyclopentadienylcobalt linear [4]phenylene complexes, J. Mol. Model. 19 (2013) 1779–1787.
[28] M.J. Lee, M. Balanay, D. Kim, Molecular design of distorted push–pull porphyrins for dye-sensitized solar cells, Theor. Chem. Acc. 131 (2012) 1–12.
[29] A. Alparone, Comparative study of CCSD(T) and DFT methods: electronic (hyper)polarizabilities of glycine, Chem. Phys. Lett. 514 (2011) 21–25.
[30] B. Champagne, E. Botek, M. Nakano, T. Nitta, K. Yamaguchi, Basis set and electron correlation effects on the polarizability and second hyperpolarizability of model open-shell π-conjugated dimers, J. Chem. Phys. 122 (2005) 114315 (1–12).
[31] M. Nakano, R. Kishi, T. Nitta, T. Kubo, K. Nakasuji, K. Kamada, Second hyperpolarizability (γ) of singlet diradical system: dependence of γ on the diradical character, J. Phys. Chem. A 109 (2005) 885–891.
[32] Y. Zhao, D. Truhlar, The M06 suite of density functionals for main group thermochemistry, thermochemical kinetics, noncovalent interactions, excited states, and transition elements: two new functionals and systematic testing of four M06-class functionals and 12 other functionals, Theor. Chem. Acc. 120 (2008) 215–241.
[33] V. Barone, O. Crescenzi, R. Improta, Computation of spectroscopic parameters in vacuo and in condensed phases by methods based on the density functional theory, Quant. Struct. Act. Relat. 21 (2002) 105–118.
[34] T. Lu, F. Chen, Multiwfn: a multifunctional wavefunction analyzer, J. Comput. Chem. 33 (2012) 580–592.
[35] M.J. Frisch, G.W. Trucks, H.B. Schlegel, G.E. Scuseria, M.A. Robb, J.R. Cheeseman, Gaussian 09 D01, Gaussian Inc., Wallingford, CT, USA, 2009.
[36] K. Hatua, P.K. Nandi, Beryllium-cyclobutadiene multidecker inverse sandwiches: electronic structure and second-hyperpolarizability, J. Phys. Chem. A 117 (2013) 12581–12589.
[37] W.Y. Wang, N.N. Ma, S.L. Sun, Y.Q. Qiu, Redox control of ferrocene-based complexes with systematically extended [small π]-conjugated connectors: switchable and tailorable second order nonlinear optics, Phys. Chem. Chem. Phys. 16 (2014) 4900–4910.